Eur. Phys. J. D **35**, 527–539 (2005)
DOI: 10.1140/epjd/e2005-00211-9

THE EUROPEAN PHYSICAL JOURNAL D

Dielectric linear response of magnetized electrons: Drag force on ions

M. Walter, G. Zwicknagel[a], and C. Toepffer

Institut für Theoretische Physik II, Universität Erlangen, Staudtstr. 7, 91058 Erlangen, Germany

Received 19 November 2004 / Received in final form 1 June 2005
Published online 2nd August 2005 –

Abstract. The drag force on ions moving in a magnetized electron plasma is calculated in dielectric linear response. Various representations of the dielectric function $\varepsilon(\mathbf{k},\omega)$ are investigated for their suitability to display the limits for an infinite and a vanishing magnetic field. While the influence of the magnetic field is negligible in certain regions of $\mathbf{k}$-space, it introduces in other regions a strong oscillatory structure in the dielectric function. This requires a careful treatment of the multidimensional integrations necessary for the drag force. The contributions from oscillatory integrands are treated by the saddle point method. Explicit results are obtained for the dependence of the drag force on the magnetic field, the direction of motion of the ion relative to the magnetic field, the shielding in the electron plasma, its density and the anisotropy of the electron temperature. The importance of the collective response of the electrons is investigated for limiting cases of the magnetic field. The validity of the linearization of the dielectric theory is checked by comparison with results obtained by numerical simulation of the nonlinear Vlasov-Poisson equation. For strong magnetic fields and low ion velocities, the simulations rather agree with the complementary binary collision model than with linear response.

PACS. 34.50.Bw Energy loss and stopping power – 41.20.-q Applied classical electromagnetism – 52.20.-j Elementary processes in plasmas – 52.40.Mj Particle beam interactions in plasmas

1 Introduction

The energy loss of charged particles in matter has been studied intensively since ninety years starting from the fundamental papers by Bohr [1], Bethe [2] and Bloch [3]. There are basically two complementary approaches: In the dielectric theory (DT), see, for example [4,5], the projectile is decelerated by the polarization cloud it creates in its wake. This is a continuum treatment in which the response of the target to the projectile as external perturbation is calculated. The collectivity of this response can be taken into account. Cut-offs are required to exclude hard collisions between close particles. In the binary collision approximation (BC), on the other hand, the energy loss of the projectile is the aggregate of subsequent, isolated pairwise interactions with the target particles, see e.g. [6]. This requires cut-offs at large distances to account for shielding. Except for nuclear stopping at the lowest particle velocities important features of the stopping process can already be studied by considering the drag which an electron plasma exerts on an ion. Moreover, this is realistic for important applications: The phase space quality of ion beams in storage rings can be improved by electron cooling [7–10]. In traps heavy ions are cooled by electrons for precision tests of QED [11] and antiprotons are cooled by electrons and positrons to produce cold antihydrogen [12,13] with the ultimate aim of CPT tests. However, in these applications the particles move in strong magnetic fields, which imposes formidable problems in both the binary collision model and in the linearized dielectric theory. In BC the problem of two charged particles cannot be solved in a closed form any more, as the magnetic field prevents a separation of the relative motion and the motion of the center mass. In the linear response (LR) approximation to the DT there exist closed expressions for the dielectric function $\varepsilon(\mathbf{k},\omega)$ [14,15], but the magnetic field introduces a strongly oscillatory structure in the $\mathbf{k}$-integral required for the drag force. A practicable expression in form of a one-dimensional integral has been derived for the limiting case of an infinite magnetic field [15]. It is the aim of this paper to calculate the drag force without limiting assumptions on the strength of the magnetic field and the direction of the ion's motion relative to the magnetic field. For that purpose we introduce a simplification in the integrand for the drag which in physical terms amounts to a replacement of the dynamic collective response of the electrons by a static response, e.g. a shielding of the electron-ion interaction.

The paper is organized as follows: in Section 2 we briefly derive the LR for the drag force and discuss two equivalent representations for the dielectric function in an

[a] e-mail: zwicknagel@theorie2.physik.uni-erlangen.de

integral form suitable to discuss the transition to weak magnetic fields $B \to 0$ [15] and in terms of Bessel functions [14] which is more suitable for a numerical evaluation. In Section 3 we present results for the dependence of the drag force on the strength of the magnetic field B, the direction of motion of the ion relative to $\mathbf{B}$, the shielding in the electron plasma, its density and the anisotropy of its temperature distribution. The simplified linearized dielectric theory is compared in Section 4 with other treatments. In certain limiting cases the dynamic collectivity in the response of the electrons has been included [8,9,15], this allows to estimate the error introduced by the static approximation. Much more important is the failure of the linearization of the dielectric theory which is demonstrated by comparing with results from a numerical solution of the underlying nonlinear Vlasov-Poisson equation. For large magnetic fields and low ion velocities these agree rather with the complementary BC model. These discrepancies can be traced to the different cut-off procedures employed in the DT and the BC, respectively.

2 The dielectric linear response theory (LR, DT)

2.1 The dielectric function

In the dielectric theory (DT) one calculates the polarization of the medium, here the magnetized electrons, due to an external perturbation, here the ion. For the derivation of the dielectric function we follow first the treatment of Ichimaru [14], and put then special emphasis on the origin of problems in the evaluation of the drag force. The electron distribution function $f(\mathbf{r},\mathbf{v},\mathbf{t})$ is the solution of the Vlasov equation

$$\frac{df(\mathbf{r},\mathbf{v},\mathbf{t})}{dt} = \frac{\partial f}{\partial t} + \mathbf{v}\cdot\frac{\partial f}{\partial \mathbf{r}} + \frac{\mathbf{F}}{m}\cdot\frac{\partial f}{\partial \mathbf{v}} = 0 \tag{2.1}$$

where

$$\mathbf{F}(\mathbf{r},\mathbf{v},\mathbf{t}) = -e(\mathbf{E}(\mathbf{r},\mathbf{t}) + \mathbf{v}\times\mathbf{B}) \tag{2.2}$$

is the force on the electrons with charge $-e$, mass m and velocity $\mathbf{v}$. In the present application the magnetic field is homogeneous and the coordinate system will be oriented according to $\mathbf{B} = B\mathbf{e}_z$. The electric field is $\mathbf{E} = -\nabla\Phi = -\nabla\Phi_i - \nabla\Phi_{\rm pol}$ with the potential

$$\Phi_i = \frac{Ze}{4\pi\varepsilon_0|\mathbf{r}-\mathbf{v}_i t|} \tag{2.3}$$

due to the perturbing ion with charge Ze and velocity $\mathbf{v}_i$ and the polarization potential which is related to the electron density $n(\mathbf{r},t) = \int d^3v f(\mathbf{r},\mathbf{v},\mathbf{t})$ by the Poisson equation

$$\Delta\Phi_{\rm pol} = \frac{en_{\rm pol}(\mathbf{r},t)}{\varepsilon_0} = \frac{e}{\varepsilon_0}(n(\mathbf{r},t)-n_0) = \frac{e}{\varepsilon_0}\left(\int d^3v f(\mathbf{r},\mathbf{v},t) - n_0\right). \tag{2.4}$$

Here ε_0 is the permittivity of the vacuum and n_0 is the homogeneous bulk density of the electrons. As the Vlasov-Poisson system (2.1), (2.4) is nonlinear in the electron distribution an exact, self-consistent solution can only be obtained numerically, see below.

After Fourier transformation the total potential Φ, the polarization potential $\Phi_{\rm pol}$ and the potential Φ_i due to the ion are related in linear response by

$$\varepsilon(\mathbf{k},\omega)\tilde{\Phi}(\mathbf{k},\omega) = \tilde{\Phi}_i(\mathbf{k},\omega)$$

and

$$\tilde{\Phi}_i(\mathbf{k},\omega) = \tilde{\Phi}(\mathbf{k},\omega) - \tilde{\Phi}_{\rm pol}(\mathbf{k},\omega) = \tilde{\Phi}(\mathbf{k},\omega) - \frac{e\tilde{n}_{\rm pol}(\mathbf{k},\omega)}{\varepsilon_0 k^2} = \tilde{\Phi}(\mathbf{k},\omega) - \frac{e}{\varepsilon_0 k^2}\int d^3v \tilde{f}_1(\mathbf{k},\mathbf{v},\omega) \tag{2.5}$$

where the dielectric function $\varepsilon(\mathbf{k},\omega)$ is defined by the first equation and (2.4) has been used in the third equation.

The first order perturbation $\tilde{f}_1$ is obtained by integration along the unperturbed trajectories, see e.g. reference [14] for details. It is proportional to $\mathbf{E}(\mathbf{k},\omega) = -i\mathbf{k}\tilde{\Phi}(\mathbf{k},\omega)$. Inserting $\tilde{f}_1$ into definition (2.5) results in

$$\varepsilon(\mathbf{k},\omega) = 1 - i\frac{\omega_p^2}{n_0 k^2}\int d^3v \left(\mathbf{k}\cdot\frac{\partial f_0(\mathbf{v})}{\partial \mathbf{v}}\right) H(\mathbf{k},\mathbf{v},\omega) \tag{2.6}$$

with the equilibrium distribution f_0 and the plasma frequency $\omega_p = (e^2 n_0/m\varepsilon_0)^{\frac{1}{2}}$. Here the function

$$H(\mathbf{k},\mathbf{v},\omega) = \int_0^\infty d\tau \exp\left[-i(\mathbf{k}\cdot R(\tau)\mathbf{v} - (\omega+i0^+)\tau)\right] \tag{2.7}$$

with

$$R(\tau) = \frac{1}{\omega_c}\begin{pmatrix} \sin\omega_c\tau & \cos\omega_c\tau - 1 & 0 \\ 1-\cos\omega_c\tau & \sin\omega_c\tau & 0 \\ 0 & 0 & \omega_c\tau \end{pmatrix}$$

and the cyclotron frequency $\omega_c = eB/m$ accounts for the unperturbed helical motion of the electrons with $\mathbf{r}(t') = \mathbf{r}(t) + R(t'-t)\cdot\mathbf{v}(t)$. The τ-integration is facilitated by using the axial symmetry about the z-axis. We choose $\mathbf{k} = k_\perp\mathbf{e}_x + k_\parallel\mathbf{e}_z$ and $\mathbf{v} = v_\perp(\cos\varphi\mathbf{e}_x + \sin\varphi\mathbf{e}_y) + v_\parallel\mathbf{e}_z$ so that

$$H(\mathbf{k},\mathbf{v},\omega) = \int_0^\infty d\tau \exp\left[-i\left\{\frac{k_\perp v_\perp}{\omega_c}(\sin(\omega_c\tau+\varphi) - \sin\varphi) + k_\parallel v_\parallel\tau - (\omega+i0^+)\tau\right\}\right]. \tag{2.8}$$

2.2 Representation as sum over Bessel functions

For the τ-integration a representation of the exponential by an infinite sum of Bessel functions is inserted

$$H(\mathbf{k},\mathbf{v},\omega) = \sum_{l,n=-\infty}^{\infty} J_l(\kappa')J_n(\kappa')e^{-i(l-n)\varphi} \times \int_0^{\infty} d\tau \exp\left[-i(k_\parallel v_\parallel + l\omega_c) - (\omega + i0^+)\tau\right] = i\sum_{l,n=-\infty}^{\infty} \frac{J_l(\kappa')J_n(\kappa')e^{-i(l-n)\varphi}}{\omega - k_\parallel v_\parallel - l\omega_c + i0^+}. \quad (2.9)$$

This yields

$$\varepsilon(\mathbf{k},\omega) = 1 + \frac{\omega_p^2}{n_0 k^2}\sum_{l,n=-\infty}^{\infty} J_l(\kappa')J_n(\kappa') \times \int d^3v \left(\mathbf{k}\cdot\frac{\partial f_0}{\partial \mathbf{v}}\right)\frac{e^{-i(l-n)\varphi}}{\omega - k_\parallel v_\parallel - l\omega_c + i0^+}, \quad (2.10)$$

where $\kappa' = k_\perp v_\perp/\omega_c$. In view of later application to electron cooling in storage rings we insert an anisotropic velocity distribution

$$f_0(\mathbf{v}) = f_0(v_\parallel, v_\perp) = n_0\left(\frac{m}{2\pi k_\mathrm{B}}\right)^{3/2}\frac{1}{T_\perp T_\parallel^{\frac{1}{2}}} \times \exp\left(-\frac{v_\perp^2}{2v_{\mathrm{th}\perp}^2}\right)\exp\left(-\frac{v_\parallel^2}{2v_{\mathrm{th}\parallel}^2}\right). \quad (2.11)$$

Here k_B is the Boltzmann constant and the thermal velocities $v_{\mathrm{th}\perp,\parallel}$ are related to the temperatures $T_{\perp,\parallel}$ transverse and parallel to the magnetic field (z-direction) by $v_{\mathrm{th}\perp,\parallel} = (k_\mathrm{B}T_{\perp,\parallel}/m)^{\frac{1}{2}}$, respectively. The velocity integrations can be done in cylindrical coordinates. The result can be expressed in terms of modified Bessel functions I_l [16] and the plasma dispersion function W [14]

$$\varepsilon(\mathbf{k},\omega) = 1 + \frac{e^{-\kappa}}{\lambda_{\mathrm{D}\parallel}^2 k^2}\sum_{l=\infty}^{\infty} I_l(\kappa) \times \left[W(z_l)\left(1 + \eta\frac{l\omega_c}{\omega - l\omega_c}\right) - \eta\frac{l\omega_c}{\omega - l\omega_c}\right] \quad (2.12)$$

with

$$z_l = \frac{1}{|k_\parallel|}\frac{\omega - l\omega_c}{v_{\mathrm{th}\parallel}}, \quad \kappa = \left(\frac{k_\perp v_{\mathrm{th}\perp}}{\omega_c}\right)^2, \quad (2.13)$$

the temperature ratio $\eta = T_\parallel/T_\perp$ and the parallel Debye shielding length $\lambda_{\mathrm{D}\parallel} = v_{\mathrm{th}\parallel}/\omega_p$.

We consider first the limit of a strong magnetic field $B \to \infty$ and expand (2.12) up to the first nonvanishing order in ω_c^{-1}. While the arguments κ of the Bessel functions become small and $I_l(\kappa) \sim \kappa^l$, the arguments in the plasma dispersion function become large for $l \neq 0, W(z_l) \sim z_l^{-2}$. Thus both the Bessel and the plasma dispersion function favor the dominance of the $l = 0$ term in (2.12) for a strong magnetic field. Inserting the appropriate asymptotic expansions yields

$$\varepsilon(\mathbf{k},\omega)_{B\to\infty} \sim 1 + \frac{1}{\lambda_{\mathrm{D}\parallel}^2 k^2}(W(z_0)(1-\kappa) + \eta\kappa + O(\kappa^2)). \quad (2.14)$$

The κ-independent leading term can be obtained in a simpler one-dimensional model in which the magnetized electrons move like beads on strings [17,18].

The limit $\omega_c \to 0$ of small magnetic fields requires a more detailed discussion. Now $W(z_l)$ will in general not be small for $|l| \gg 1$. For the Bessel functions Ichimaru introduced an asymptotic formula valid for $l \gg 1$, $\kappa \gg 1$ and $\kappa \gg l$ [14]. Then the summation with respect to l is replaced by an integration. This can be done with some effort and there results the desired dielectric function without magnetic field [19]. These complications can be avoided by performing an expansion in terms of $\omega_c \ll 1$ before representing the function H in equation (2.8) by Bessel functions.

2.3 Integral representation

For the purpose of performing the limit $B \to 0$ analytically, it turns out to be even more advantageous to use an integral representation for the dielectric function [15] which is equivalent to equation (2.12)

$$\varepsilon(\mathbf{k},\omega) = 1 + \frac{1}{k^2\lambda_{\mathrm{D}\parallel}^2}\left[1 + is\sqrt{2}\int_0^{\infty} dt \exp(ist\sqrt{2} - X(t)) \times \left\{1 + \frac{kv_{\mathrm{th}\parallel}}{is\omega_c}\sin^2\vartheta\left(1 - \frac{1}{\eta}\right)\sin\left(\frac{\omega_c t\sqrt{2}}{kv_{\mathrm{th}\parallel}}\right)\right\}\right] \quad (2.15)$$

with $s = \omega/(kv_{\mathrm{th}\parallel}), \vartheta = \sphericalangle(\mathbf{k},\mathbf{B})$ and

$$X(t) = t^2\cos^2\vartheta + \frac{k^2 v_{\mathrm{th}\perp}^2}{\omega_c^2}\sin^2\vartheta\left[1 - \cos\left(\frac{\omega_c t\sqrt{2}}{kv_{\mathrm{th}\parallel}}\right)\right]. \quad (2.16)$$

In the limit of small magnetic fields one expands here the trigonometric functions up to second order and does the t-integration. There results

$$\lim_{B\to 0}\varepsilon(\mathbf{k},\omega) = 1 + \frac{1}{\lambda_{\mathrm{D}\parallel}^2 k_\eta^2}W\left(\frac{\omega}{k_\eta v_{\mathrm{th}\parallel}}\right) \quad (2.17)$$

with $k_\eta^2 = \eta^{-1}k_\perp^2 + k_\parallel^2$. In the subsequent numerical work the representation (2.12) will also be used for weak magnetic fields.

2.4 Drag force

Due to their polarization the electrons exert a drag on an ion with charge Ze moving with velocity $\mathbf{v}_i$

$$\mathbf{F} = -Ze\left(\nabla\Phi_{\mathrm{pol}}\right)_{\mathbf{r}=\mathbf{v}_i t} \quad (2.18)$$

and the energy loss of the ion is $dE/ds = \hat{\mathbf{v}}_i \cdot \mathbf{F}$. The polarization potential is obtained from equation (2.5)

$$\Phi_{\rm pol}(\mathbf{r},t) = \frac{Ze}{(2\pi)^3\varepsilon_0}\int d^3k \left(\frac{1}{\varepsilon(\mathbf{k},\mathbf{k}\cdot\mathbf{v}_i)}-1\right)\frac{e^{i\mathbf{k}(\mathbf{r}-\mathbf{v}_i t)}}{k^2}. \quad (2.19)$$

With the help of the relation $\varepsilon^*(\mathbf{k},\mathbf{k}\cdot\mathbf{v}_i) = \varepsilon(-\mathbf{k},-\mathbf{k}\cdot\mathbf{v}_i)$ and $\omega = \mathbf{k}\cdot\mathbf{v}_i$ the drag force can be written as

$$\mathbf{F} = \frac{1}{(2\pi)^3}\int d^3k\mathbf{k}\ \frac{\varepsilon_0 k^2}{e^2}|\tilde{V}(\mathbf{k})|^2 {\rm Im}\left(\frac{1}{\varepsilon(\mathbf{k},\omega)}\right) = \frac{-1}{(2\pi)^3}\int d^3k\mathbf{k}\ \frac{\varepsilon_0 k^2}{e^2}|\tilde{V}(\mathbf{k})|^2\frac{{\rm Im}\varepsilon(\mathbf{k},\omega)}{|\varepsilon(\mathbf{k},\omega)|^2} \quad (2.20)$$

where $\tilde{V}(\mathbf{k}) = -Ze^2/(\varepsilon_0 k^2)$ is the ion-electron potential energy. The complicated structure of the dielectric function (2.12) prevents any closed evaluation of the $\mathbf{k}$-integral unless one assumes a completely flattened electron distribution function [8] or an infinite magnetic field [15]. For general cases we propose an approximation in which the effective, dynamic ion-electron interaction is replaced by a statically screened interaction according to

$$\tilde{V}(\mathbf{k})/|\varepsilon(\mathbf{k},\omega)| \longrightarrow \tilde{V}(\mathbf{k})/|\varepsilon(\mathbf{k},0)| = \tilde{U}(\mathbf{k}) \approx -\frac{Ze^2}{\varepsilon_0(k^2+\beta^2)}. \quad (2.21)$$

In this approximation the electron-electron interaction is neglected except for a collective static shielding of the ion, which is described by a parameter β

$$U(\mathbf{r}) = -\frac{Ze^2}{4\pi\varepsilon_0 r}\exp(-\beta r). \quad (2.22)$$

As usual in the linearization of the DT the k-integral in equation (2.20) must be cut off at large wave numbers in order to exclude hard collisions. Here we use cylindrical coordinates $\mathbf{k} = (k_\perp\cos\varphi, k_\perp\sin\varphi, k_\parallel)$ and cut the integrations with respect to $k_\perp$ and $k_\parallel$ at $k_{m\perp}$ and $k_{m\parallel}$, respectively. Insertion of equation (2.21) into equation (2.20) yields then

$$\mathbf{F} = -\frac{Z^2e^2}{(2\pi)^{5/2}\varepsilon_0}\frac{2}{\lambda_{D\parallel}v_{\rm th\parallel}}\int_0^{k_{m\perp}} dk_\perp k_\perp \int_0^{k_{m\parallel}} dk_\parallel \int_0^{\pi} d\varphi \times(k_\perp\cos\varphi,0,k_\parallel)\frac{e^{-\kappa}}{|k_\parallel|(k^2+\beta^2)^2} \times \sum_{l=-\infty}^{\infty} I_l(\kappa)\exp\left(-\frac{(\omega-l\omega_c)^2}{2v_{\rm th\parallel}^2k_\parallel^2}\right)(\omega-l\omega_c(1-\eta)). \quad (2.23)$$

It is assumed that the ion moves in the $x-z$-plane so that $\omega = \mathbf{k}\cdot\mathbf{v}_i = k_\perp v_{i\perp}\cos\varphi + k_\parallel v_{i\parallel}$. In view of the dominance of the $l = 0$ term in the limit $B\to\infty$ we exhibit its contribution separately

$$\mathbf{F} = \mathbf{F}_0 + \mathbf{F}_l$$

with

$$\mathbf{F}_0 = -A\int_0^{k_{m\perp}} dk_\perp k_\perp \int_0^{k_{m\parallel}} dk_\parallel \int_0^{\pi} d\varphi\,(k_\perp\cos\varphi,0,k_\parallel) \times \frac{e^{-\kappa}I_0(\kappa)\omega}{k_\parallel(k^2+\beta^2)^2}\exp\left(-\frac{\omega^2}{2v_{\rm th\parallel}^2k_\parallel^2}\right) \quad (2.24)$$

and

$$A = \frac{Z^2e^2}{(2\pi)^{5/2}\varepsilon_0}\ \frac{2}{\lambda_{D\parallel}^2 v_{\rm th\parallel}}.$$

Expanding for large magnetic fields up to order $O(\omega_c^{-2})$ yields

$$\mathbf{F}\propto\mathbf{F}_0 = -A\int_0^{k_{m\perp}} dk_\perp k_\perp \int_0^{k_{m\parallel}} dk_\parallel \int_0^{\pi} d\varphi(k_\perp\cos\varphi,0,k_\parallel) \times\frac{\omega(1-\kappa)}{k_\parallel(k^2+\beta^2)^2}\exp\left(-\frac{\omega^2}{2v_{\rm th\parallel}^2k_\parallel^2}\right). \quad (2.25)$$

Of particular interest is here the longitudinal drag for $\mathbf{v}_i = v_i\hat{\mathbf{e}}_z$, in which the $\mathbf{k}$-integral can be done in closed form [19]

$$F_{0\parallel} = \mathbf{F}_0\cdot\hat{\mathbf{e}}_z = \frac{A}{4}\pi v_i\exp\left(-\frac{v_i^2}{2v_{\rm th\parallel}^2}\right) \times\left\{\ln\left[\frac{(k_{m\perp}^2+\beta^2)(k_{m\parallel}^2+\beta^2)}{\beta^2(k_{m\parallel}^2+k_{m\perp}^2+\beta^2)}\right]\left(1+\beta^2\frac{v_{\rm th\perp}^2}{\omega_c^2}\right) -k_{m\parallel}^2\frac{v_{\rm th\perp}^2}{\omega_c^2}\ln\left[1+\frac{k_{m\perp}^2}{k_{m\parallel}^2+\beta^2}\right]\right\} \quad (2.26)$$

which does not vanish. This is in contradiction to the binary collision (BC) model [20], where the electrons move for $B\to\infty$ like beads on a wire and no energy can be transferred between them and a positively charged longitudinally moving ion for reason of symmetry.

We turn now to the limit of small ion velocities $v_i \ll v_{\rm th\parallel}$. Without magnetic field the energy loss depends linearly on v_i [21,22]. In the presence of a magnetic field there occurs an anomaly [15] as soon as $\alpha = \sphericalangle(\mathbf{v}_i,\mathbf{B}) \neq 0$: inserting $\omega = \mathbf{k}\cdot\mathbf{v}_i = v_i(k_\perp\cos\varphi\sin\alpha + k_\parallel\cos\alpha)$ into $\mathbf{F}_0$ the energy loss has a contribution

$$\left(\frac{dE}{ds}\right)_0 = \mathbf{F}_0\cdot\hat{\mathbf{v}}_i = -Av_i\int_0^{k_{m\perp}} dk_\perp k_\perp \int_0^{\pi} d\varphi \int_0^{k_{m\parallel}} dk_\parallel \times\frac{(k_\perp\cos\varphi\sin\alpha + k_\parallel\cos\alpha)^2}{k_\parallel(k^2+\beta^2)^2} \times e^{-\kappa}I_0(\kappa)\exp\left(-\frac{\omega^2}{2v_{\rm th\parallel}^2k_\parallel^2}\right) \quad (2.27)$$

which turns out to be logarithmic. This anomalous behaviour results from integrals in (2.27) with the structure

$$\Lambda \sin\alpha \int_0^{k_{m\parallel}} dk_\parallel k_\parallel^{-1} \exp(-\Lambda^2/k_\parallel^2) = \frac{1}{2}\Lambda \sin\alpha \left(-\gamma - \ln\frac{\Lambda^2}{k_{m\parallel}^2}\right). \quad (2.28)$$

Here γ is Euler's constant and

$$\Lambda = \frac{v_i \sin\alpha}{v_{\mathrm{th}\parallel}} = \frac{v_{i\perp}}{v_{\mathrm{th}\parallel}}. \quad (2.29)$$

A detailed discussion shows that the $l = 0$ contribution to the energy loss for small ion velocities is [19]

$$\left(\frac{dE_i}{ds}\right)_0 \propto \frac{v_{i\perp}}{v_{\mathrm{th}\parallel}} \left\{ \left(\ln\frac{v_{\mathrm{th}\parallel}}{v_{i\perp}} + \tilde{\gamma} \right) \mathrm{I1} - \mathrm{I2} + \mathrm{I3}\frac{\cos^2\alpha}{\sin\alpha} \right\}. \quad (2.30)$$

where $\tilde{\gamma} = (3\ln 2 - \gamma - 1)/2$ and I1–I3 are certain integrals with respect to $k_\perp$ which still depend logarithmically on the upper boundaries $k_{m\perp}$ and $k_{m\parallel}$.

3 Results

The drag force is calculated numerically from the integrals (2.23). This requires a physically motivated choice of the cutoff parameters k_m and the shielding parameter β. Furthermore it is useful to introduce a scaling to dimensionless quantities. The magnetic field introduces a complicated structure into the dielectric function (2.12) which poses a challenge for the integrations in (2.23).

3.1 Cutoff and shielding parameters

Without magnetic field the linearized DT yields Debye-Hückel shielding for an isotropic, weakly coupled plasma, $\beta = \lambda_D^{-1}$. In the general case the shape of the shielding cloud depends on the temperature anisotropy, the strength of the magnetic field and the direction of the ion velocity in an involved manner. For weak magnetic fields $\omega_c \ll \omega_p$ and small velocities the shielding length is $\lambda \geq \lambda_{D\parallel}$ in the longitudinal and $\lambda \leq \lambda_{D\perp}$ in the transverse direction. Here we will use an effective isotropic shielding with $\beta = \overline{\lambda}_D^{-1}$, where $\overline{\lambda}_D$ is calculated with the mean temperature $\overline{T} = \frac{1}{3}T_\parallel + \frac{2}{3}T_\perp$. An analogous procedure is adapted for the cutoff k_m [22] by which hard collisions are excluded

$$k_{m\perp} = k_{m\parallel} = k_m = \frac{2 + (v_i/\overline{v}_{\mathrm{th}})^2}{\sqrt{3}|Z|\overline{\Gamma}^{3/2}\overline{\lambda}_D}. \quad (3.1)$$

Here $\overline{v}_{\mathrm{th}} = (k_\mathrm{B}\overline{T}/m)^{\frac{1}{2}}$ and

$$\overline{\Gamma} = \frac{e^2}{4\pi\varepsilon_0 a k_\mathrm{B}\overline{T}} \quad (3.2)$$

is the (mean) plasma parameter with the mean distance $a = (3/(4\pi n_0))^{\frac{1}{3}}$ between the electrons.

We will discuss the influence of this choice of β and k_m on the drag force in Section 3.6 below.

3.2 Scaling

Dimensionless quantities will be introduced by scaling with the longitudinal temperature $T_\parallel$, i.e.

$$[r] = r/\lambda_{D\parallel} \quad (3.3)$$

for lengths

$$[v] = v/v_{\mathrm{th}\parallel} \quad (3.4)$$

for velocities and for the drag

$$[F] = \frac{\Gamma_\parallel a}{3k_\mathrm{B}T_\parallel} F \quad (3.5)$$

with the longitudinal plasma parameter $\Gamma_\parallel = \overline{\Gamma}\ \overline{T}/T_\parallel$. The frequencies are measured in units of the plasma frequency

$$[\omega] = \omega/\omega_p. \quad (3.6)$$

Dropping the square indicating scaled quantities the drag force (2.23) becomes

$$\mathbf{F} = -\frac{2Z^2\Gamma_\parallel^3}{\pi^2} \int_0^{k_{m\perp}} dk_\perp k_\perp \int_0^{k_{m\parallel}} dk_\parallel \int_0^{\pi} d\varphi \times (k_\perp\cos\varphi, 0, k_\parallel)\frac{k^2}{(k^2+\beta^2)^2}\ \mathrm{Im}(\varepsilon(\mathbf{k},\omega)). \quad (3.7)$$

Here

$$\mathrm{Im}\ \varepsilon(\mathbf{k},\omega) = \sqrt{\frac{\pi}{2}}\frac{e^{-\kappa}}{k^2|k_\parallel|}\sum_{l=-\infty}^{\infty} I_l(\kappa)\exp\left(-\frac{(\omega - l\omega_c)^2}{2k_\parallel^2}\right) \times (\omega - l\omega_c(1-\eta)) \quad (3.8)$$

is the imaginary part of the dielectric function. Because of equations (2.13) and (3.4) the argument of the Bessel function is now

$$\kappa = \frac{1}{\eta}(k_\perp/\omega_c)^2. \quad (3.9)$$

The limits of (3.8) for weak and strong magnetic fields are

$$\lim_{B\to 0}\mathrm{Im}\,\varepsilon(\mathbf{k},\omega) = \sqrt{\frac{\pi}{2}}\ \frac{\omega}{k_\eta^3}\exp\left(-\frac{\omega^2}{2k_\eta^2}\right) \quad (3.10)$$

and

$$\lim_{B\to\infty}\mathrm{Im}\,\varepsilon(\mathbf{k},\omega) = \sqrt{\frac{\pi}{2}}\ \frac{\omega}{k^2|k_\parallel|}\,(1-\kappa)\ \exp\left(-\frac{\omega^2}{2k_\parallel^2}\right). \quad (3.11)$$

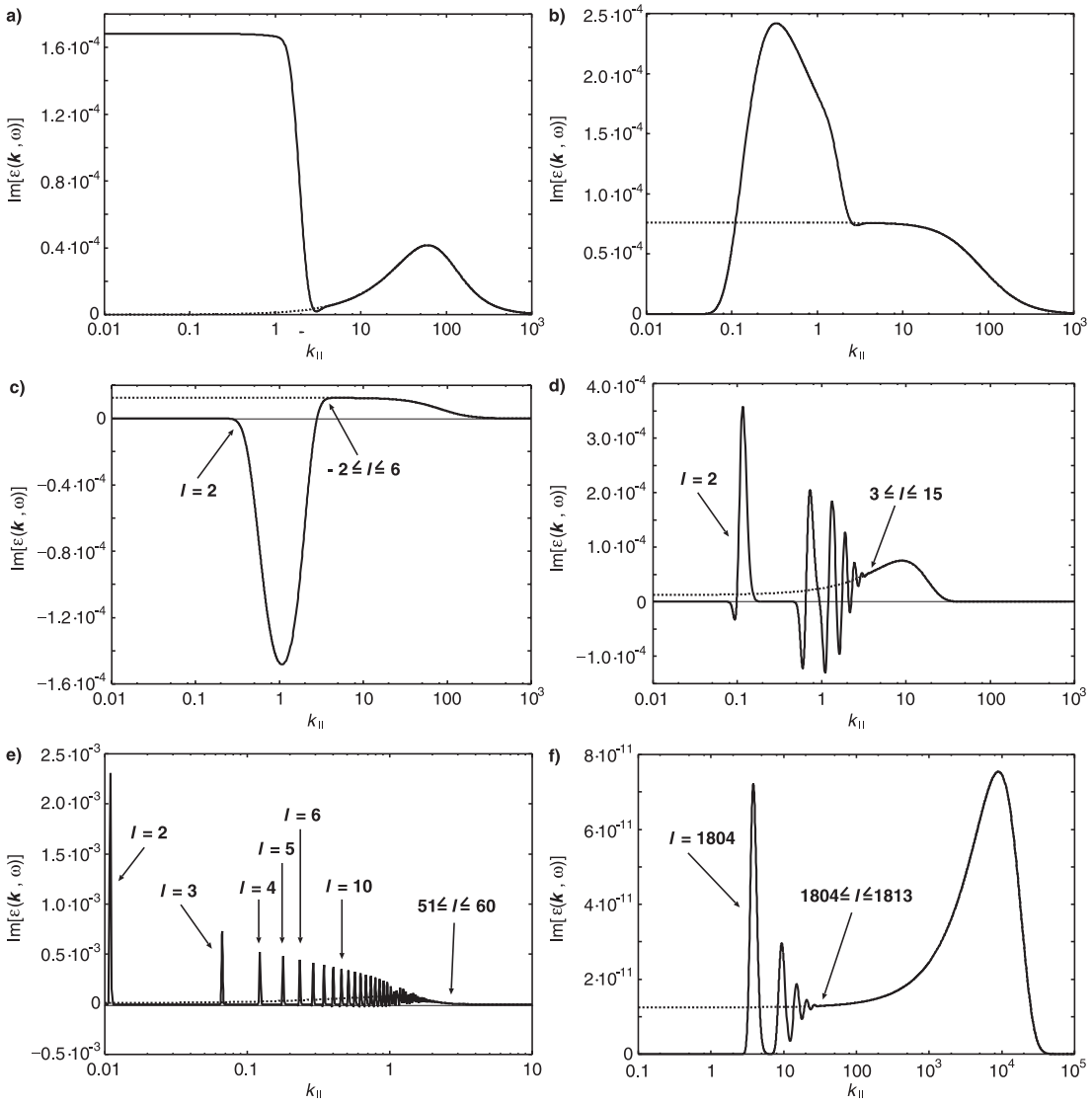

Fig. 1. The imaginary part of the dielectric function with (solid curves) and without magnetic field (dotted curves) as function of $k_\parallel$. The other variables and parameters are chosen according to Table 1. Some prominent structures are labelled by the dominantly contributing values of l in the summation (3.8).

3.3 Structure of the dielectric function and saddle point approximation

Inspection shows that the integrand in (3.7) has only integrable singularities [19], but the structure of the dielectric function (3.8) renders the numerical integration complicated. The problems arise from the maxima of the Gaussian under the l-summation in equation (3.8). If the slope of $(\omega - l\omega_c)/k_\parallel$ is large about its zeroes, the maxima can be very sharp. Moreover such sharp maxima of the integrand in equation (3.7) can lie very close. On the other hand the influence of the magnetic field becomes negligible for large values of $k_\parallel$, so that equation (3.8) for the dielectric function at arbitrary strengths of the magnetic field can be replaced by the much simpler expression (3.10) for a vanishing field. Typical examples of the dependence of $\mathrm{Im}\varepsilon(\mathbf{k},\omega)$ on $k_\parallel$ are shown in Figure 1 for the fixed values of $k_\perp, v_{i\perp}\cos\varphi, v_{i\parallel}, \omega_c$ and η given in Table 1. The sharp maxima in the solid curves for finite B are labelled by the dominantly contributing values of l. For large values of $k_\parallel \gg 1$ any peaks disappear and the results for finite values of B merge with

Table 1. Scaled parameters and variables for Figure 1.

panel	$k_\perp$	$v_{i\perp}\cos\varphi$	$v_{i\parallel}$	ω_c	η
a	10.0	0.0	1.0	5.546	0.01
b	10.0	10.0	1.0	5.546	0.01
c	10.0	1.0	0.0	5.546	0.01
d	10.0	1.0	10.0	5.546	0.01
e	10.0	1.0	100.0	5.546	0.01
f	10^5	1.0	10.0	55.46	0.01

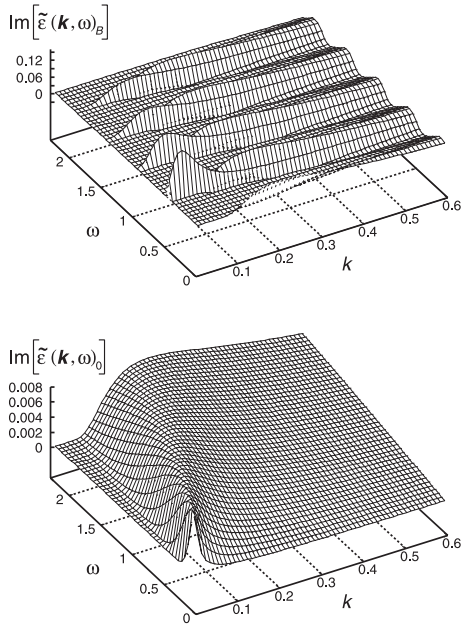

Fig. 2. 3-d plots of $k^2\mathrm{Im}\varepsilon(\mathbf{k},\omega)$ (top panel for a finite magnetic field, bottom panel for a vanishing magnetic field). Other parameters according to Table 2.

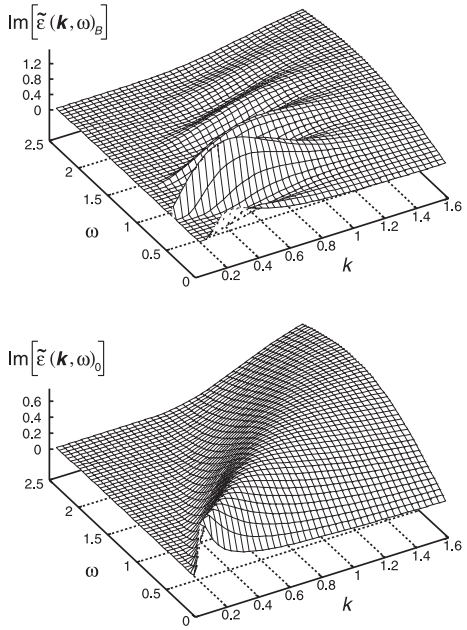

Fig. 3. The same as in Figure 2.

the smooth, dotted curves obtained from equation (3.10) for $B = 0$. As the dielectric function diverges for $\omega > 0$ and $k \to 0$ we consider $\tilde{\varepsilon}(\mathbf{k},\omega)_{B,0} = k^2\varepsilon(\mathbf{k},\omega)_{B,0}$. Here the subscripts B and 0 indicate the presence or absence of a magnetic field, respectively. In Figures 2–4 we show plots of $\mathrm{Im}\tilde{\varepsilon}(\mathbf{k},\omega)_{B,0}$ as function of ω and k for various $\theta = \sphericalangle(\mathbf{k},\hat{\mathbf{e}}_z)$ and temperature anisotropies η and $\omega_c = 0.5$. For $\theta = 80°$, i.e. $k_\parallel < k_\perp$ one expects ridges in $\mathrm{Im}\tilde{\varepsilon}(\mathbf{k},\omega)_B$ which run parallel to the k-axis near $\omega = l\omega_c$. These are clearly visible in Figures 2 and 3. But the structure is

Table 2. Scaled parameters and variables for Figures 2–5.

Figure	θ	ω_c	η
2	80°	0.5	0.01
3	80°	0.5	1.0
4	10°	0.5	0.01
5	80°	0.05	0.01

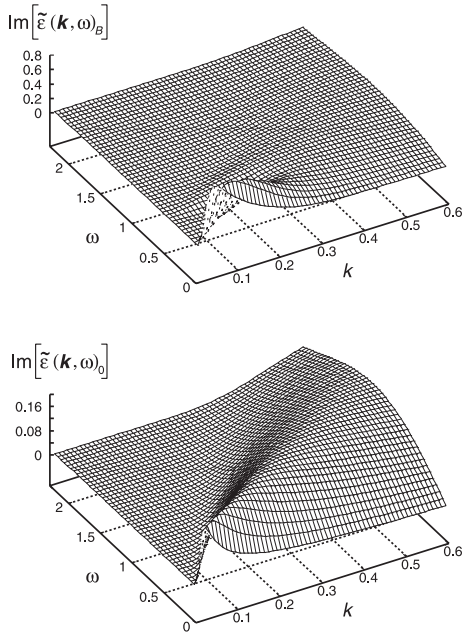

Fig. 4. The same as in Figure 2.

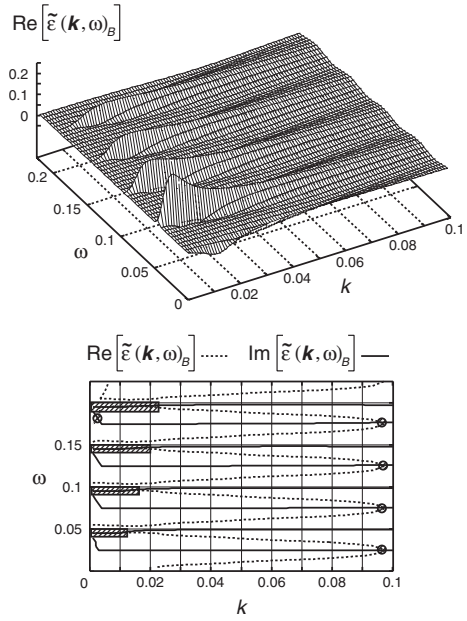

Fig. 5. Upper panel: 3-d plot of $k^2\mathrm{Re}\varepsilon(\mathbf{k},\omega)$. Lower panel: Contour plot of the zeroes of $k^2\mathrm{Re}\varepsilon(\mathbf{k},\omega)$ (dotted curves) and $k^2\mathrm{Im}\varepsilon(\mathbf{k},\omega)$ (solid curves). Areas in the (k,ω)-plane which include zeroes of both the real- and the imaginary-parts of $k^2\varepsilon(\mathbf{k},\omega)$ are shaded. Parameters according to Table 2.

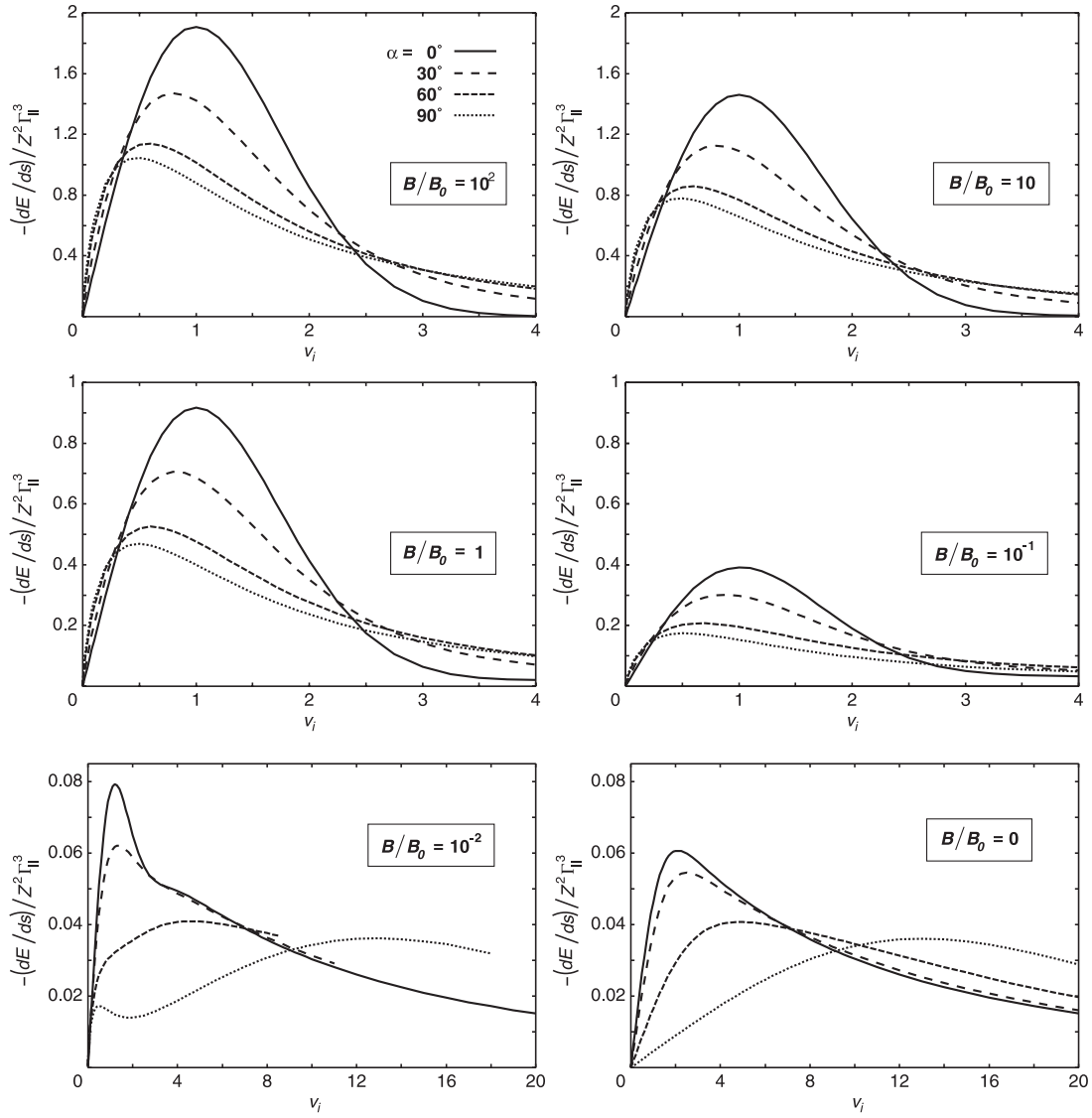

Fig. 6. Energy loss $dE/ds = \hat{\mathbf{v}}_i \cdot \mathbf{F}$ with $\mathbf{F}$ given by (3.7). Plotted is $dE/ds/(Z^2\Gamma_\parallel^3)$ in units of $3k_\mathrm{B}T_\parallel/(\Gamma_\parallel a)$ as function of v_i in units of $v_{\mathrm{th}\parallel}$ for various angles α (see panel top left) and values of the magnetic field relative to $B_0 = 50$ mT. Other parameters according to set 1 of Table 3.

also influenced by the factor $\omega - l\omega_c(1-\eta)$, which yields for the anisotropic case in Figure 2 negative values of $\mathrm{Im}\tilde{\varepsilon}(\mathbf{k},\omega)_B$ in the valleys between the ridges. Without magnetic field $\mathrm{Im}\tilde{\varepsilon}(\mathbf{k},\omega)_0$ shows a single ridge traversing the $\omega - k$ plane. For $\theta = 10°$, i.e. $k_\parallel > k_\perp$ the magnetic field has not such a pronounced influence on $\mathrm{Im}\tilde{\varepsilon}(\mathbf{k},\omega)$, as seen in Figure 4. The real part of the dielectric function is shown in Figure 5. Again there are ridges at $\omega = l\omega_c$ and negative-valued valleys in-between. Of particular interest are the dashed regions in the lower panel of Figure 5 where $\mathrm{Im}\tilde{\varepsilon}(\mathbf{k},\omega) = 0 = \mathrm{Re}\tilde{\varepsilon}(\mathbf{k},\omega)$ so that $|\varepsilon(\mathbf{k},\omega)|^2 = 0$. The analytical behaviour of the dielectric function in these regions must be known for an evaluation of the drag force according to equation (2.20).

Already the static approximation (2.21) imposes numerical challenges. Most critical is the φ-integration for which the denominator of $(\omega - l\omega_c)/k_\parallel$ becomes small for $k_\parallel \leq 1$ so that peaks occur for many combinations of the remaining integration variable $k_\perp$ and parameters $v_{i\parallel}, v_{i\perp}, \omega_c$ and η. The φ-integration is therefore done first and the peaks are treated analytically in a fifth order Laplace method [23]. The $k_\perp$-integration is done last to minimize the effort in calculating the modified Bessel functions. In the intermediate $k_\parallel$-integration the representation (3.10) is used for $k_\parallel \gtrsim 1$.

3.4 Energy loss for anisotropic velocity distributions

In Figure 6 we show the energy loss $dE/ds = \hat{\mathbf{v}}_i \cdot \mathbf{F}$ [with $\mathbf{F}$ given by (2.23), (3.7)] as function of v_i for various strengths of the magnetic field B and directions α of the

Table 3. Parameters and variables for Figures 6–13.

Set	$n_0[10^{12}\,\mathrm{m}^{-3}]$	$T_\parallel[K]$	η	B[mT]	Z
1	7.9	10	0.01	50	10
2	7.9	10	1.0	50	10
3	1.0	1.16	0.001	10^4	1
4	10^8	10^5	1.0	10^7	1
5	1.55×10^4	10	0.01	4×10^3	10

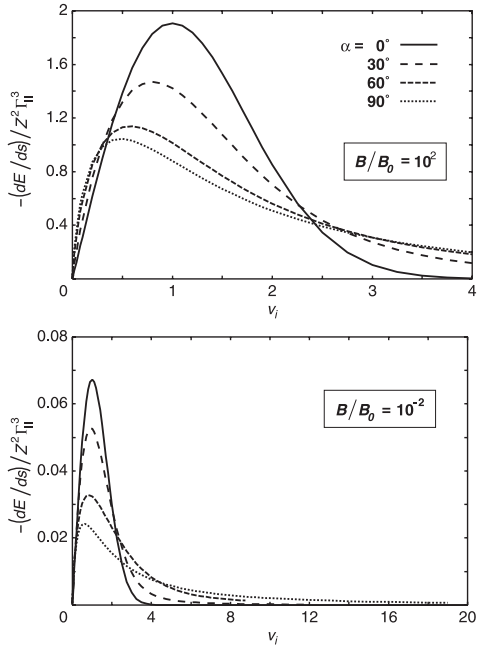

Fig. 7. The $l = 0$ contributions (2.24) to the energy loss, otherwise the same as in Figure 6.

ion velocity. For very small ion velocities $v_i \ll 1$ and $B > 0$ the energy loss grows with α due to the logarithmic contribution (2.30). However, the growth of the energy loss with α for $v_i \gtrsim 3$ is independent of the presence of a magnetic field. In the intermediate region $0.3 \lesssim v_i \lesssim 3$ a reversed behaviour can be observed, the energy loss decreases with α. For small magnetic fields the maxima of the energy loss occur at values v_i which increase with α. For large magnetic fields the motion of the electrons transverse to the field is increasingly quenched. The physical velocity scale approaches the scale (3.4) adopted for these figures. The maxima of the energy loss occur near $v_i \approx 1$ and they are ordered in a manner inverse to α. We have previously argued that the $l = 0$ contribution (2.24) to the drag is dominant for a strong magnetic field. This is clearly visible by comparing the energy loss obtained just from this term (Fig. 7) with the corresponding results in Figure 6.

As mentioned above equation (2.30) yields a logarithmic divergence in the slope of the energy loss (i.e. the friction coefficient R) for $v_i \to 0, B > 0, \alpha > 0$. The double logarithmic plot in Figure 8 shows indeed a substantial deviation between the numerical results for the drag according to equations (3.7), (3.8), the small velocity limit (2.30) on the one hand, and any linear behaviour $\propto Rv_i$ on the

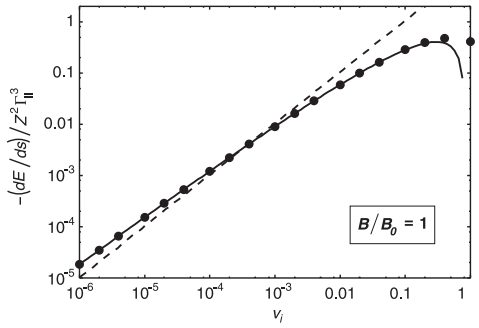

Fig. 8. Doubly logarithmic plot of the $l = 0$ contribution to the energy loss for small ion velocities for $B = B_0 = 50$ mT. The black circles result from the numerical evaluation of equation (2.24). The solid curve is the asymptotic formula (2.30), while the dashed straight line represents a linear law. Parameters according to set 1 of Table 3.

other hand. We will discuss below in Section 4 how far this anomalous behaviour and the associated large energy loss at small ion velocities and $\alpha > 0$ indicates a failure of the linearization of the DT for large magnetic fields.

3.5 Energy loss for isotropic velocity distributions

In the previous sections we considered anisotropic electron plasmas with $\eta = T_\parallel/T_\perp \ll 1$ as they occur in the cooling sections of storage rings [7–10]. In cooling traps for heavy ions or antiprotons [11–13] the electron distribution tends to be isotropic. In Figure 9 we show the dependence of the energy loss on the ion velocity for various values of α and a weak magnetic field $B = 5$ mT and a strong magnetic field $B = 5$ T as it prevails in the traps. For a weak magnetic field the direction of the ion motion hardly matters, the energy loss peaks near $v_i \approx 1.5$ for all α. For a strong magnetic field the peaks in the energy loss become smaller and are shifted towards smaller values of v_i with increasing α. For large ion velocities $v_i \gtrsim 3$ the magnetic field suppresses the energy loss and the more so, the smaller α. Comparing with Figure 6 we conclude that the influence of a temperature anisotropy decreases with growing magnetic field.

3.6 Dependence on the range and the cutoff parameter of the effective interaction

The results presented so far have been obtained with the effective ion-electron potential (2.22) whose range was chosen as the mean Debye-Hückel shielding length $\beta = \beta_0 = \overline{\lambda}_D^{-1}$. In order to get some feeling for the arbitrariness introduced by such a choice we show in Figure 10 the energy loss as function of v_i for $\beta/\beta_0 = 10, 1, 0.1$ and 0.01. Varying the range β^{-1} by a factor ten introduces just a factor ≈ 2 in the energy loss.

While the trivial dependence on the ion charge Z has been scaled away by plotting $dE/ds/(Z^2\Gamma_\parallel^3)$) there is an additional logarithmic Z-dependence due to the upper

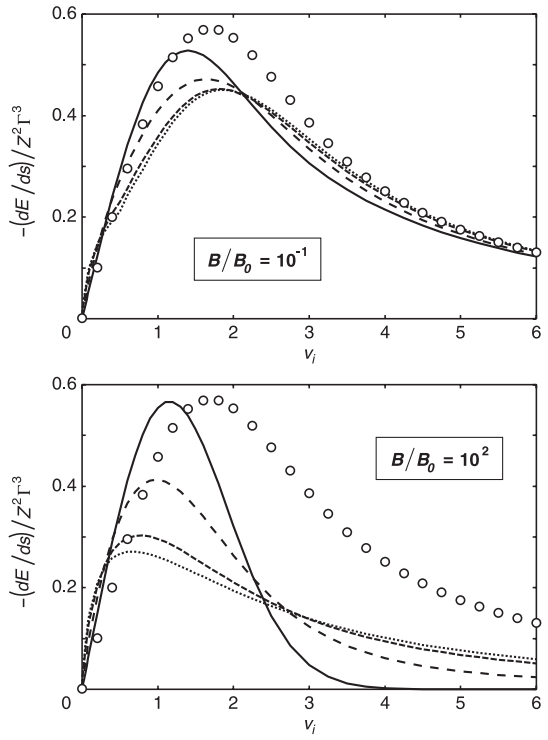

Fig. 9. The same as in Figure 6 for an isotropic plasma according to the parameter set 2 of Table 3. For comparison the energy loss without magnetic field is added (circles).

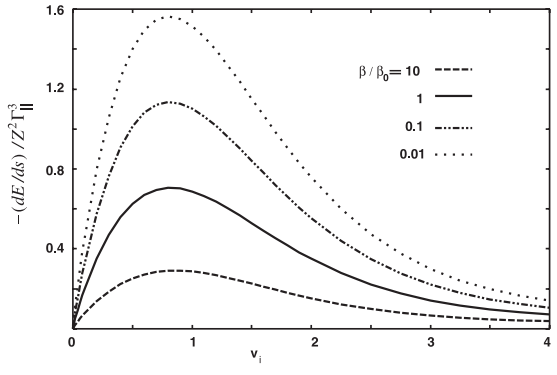

Fig. 10. Dependence of the scaled energy loss on the screening parameter β with $\beta_0 = 0.1222/\lambda_{D\|} = \overline{\lambda}_D^{-1}$. Other parameters like in set 1 of Table 3 and $\alpha = 30°$.

cutoff parameter $k_m \propto |Z|^{-1}$, see equation (3.1). In Figure 11 one sees indeed that the nontrivial dependence of the energy loss on k_m, i.e. Z, is indeed quite weak.

4 Comparison with other approaches

We will now address the role of a collective dynamic response, which was dropped in equation (2.21), the relation to the complementary binary collision (BC) model for the energy loss and the validity of the linearization of the DT in the case of strong magnetic fields.

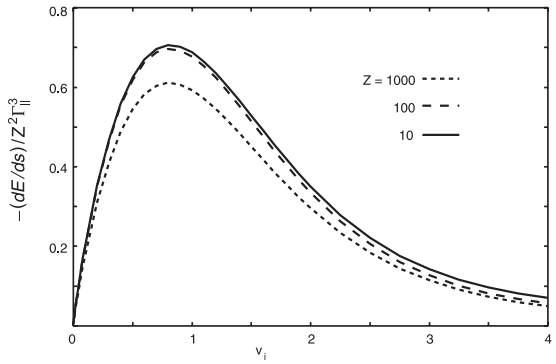

Fig. 11. Dependence of the scaled energy loss on the charge Z of the ion. Other parameters like in set 1 of Table 3 and $\alpha = 30°$.

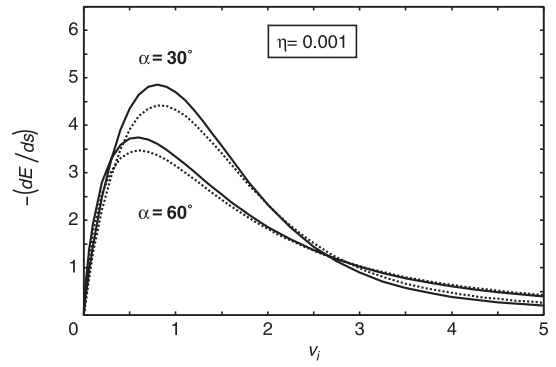

Fig. 12. The energy loss in [meV/cm] as function of the ion velocity in $v_{\mathrm{th}\|}$. Comparison of the present model with static shielding (2.21) (solid curves) with the dynamic collective theory (dotted curves) for an infinite field [15]. Parameters according to set 3 of Table 3.

4.1 Collective dynamic response

As mentioned above the integral form (2.15) of the dielectric function permits for strong magnetic fields a representation of the energy loss as a one-dimensional integral without taking the static limit $\omega \to 0$ in equation (2.21) [15]. This allows to study the importance of the dynamic collective response which was neglected up to now. The comparison in Figure 12 shows that the influence of dynamic collectivity is small in absolute terms, but becomes relatively important for large ion velocities, where the energy loss itself is small. This is confirmed by comparing with a dynamic calculation for an isotropic plasma [24]. In order to emphasize the large v_i-behaviour the energy loss was multiplied by v_i^2 in Figure 13. Again the dynamics increase the energy loss for large ion velocities, but their contribution to the total is smaller than the 50% obtained in the extreme anisotropic case with $T_\| = 0$ [8].

4.2 Binary collision model

With the replacement (2.21) one neglects the interaction between the electrons except for a static shielding of the

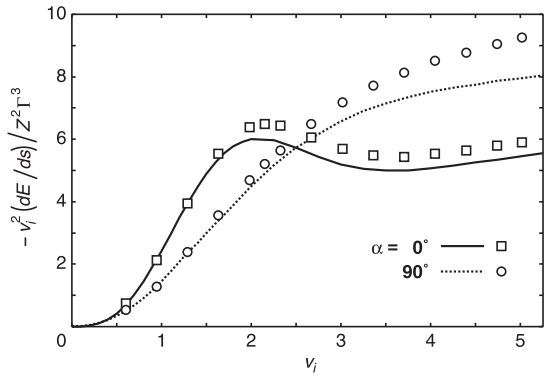

Fig. 13. Scaled energy loss as function of the scaled ion velocity. Comparison of the present model with a static shielding (2.21) (solid curve for $\alpha = 0°$, dotted curve for $\alpha = 90°$) with the dynamic collective theory (symbols) [24]. Parameters according to set 4 of Table 3.

ion-electron interaction. There results the same underlying physics as in BC with a suitably screened or cutoff interaction. Without magnetic field BC and linearized DT give indeed very close results [25]. Yet with growing magnetic field there develop increasing discrepancies between both treatments. These are particular prominent in the regime $v_i \to 0$ [20,26,27], where the linearized DT with its logarithmic singularity in the friction coefficient yields a much larger energy loss than the BC. These differences can be traced to the different cutoff procedures employed in both treatments. The cutoffs are required by the infinite range of the Coulomb interaction (BC) and its singularity at the origin (linearized DT). However, it must be noted that the order of integrations with respect to the velocity distribution on the one hand and to the ordinary (Fourier) space on the other hand is inverted: In the linearized DT the velocity averaging is performed first in the calculation of the dielectric function (2.10–2.12), the cutoff k_m in the k-integration for the drag is a velocity averaged quantity. Conversely, in BC the velocity integration is the outer one and the lower cutoff r_m excluding hard collisions in ordinary space corresponding to upper cutoff (k_m in Fourier-space) depends on the actual relative velocity between the ion and the electron. In other words, the linearized DT involves Coulomb logarithms of averages, while the BC involves averages of Coulomb logarithms [25].

For a strong magnetic field the electrons move like beads along the field lines and the BC yields a vanishing energy for comoving ions, as scattering events with a velocity transfer are prohibited for reasons of symmetry. Of course this argument holds only for the case of an attractive ion-electron potential. For a repulsive potential there occur large velocity transfers, when the particles are reflected from each other. Thus any treatment which yields results independent of the sign of the potential, like the second-order BC [20] and the linearized DT runs into difficulties. Apparently for quasi-one-dimensional motion there exists no suitable parameter of smallness so that both the linearization of DT as well as the $O(Z^2)$ perturbation expansion in the BC become doubtful. A comparison with classical trajectory Monte Carlo calculations [27,28] shows that this can be healed in BC for attractive potentials by introducing a modified, self-cutting Coulomb logarithm accounting for hard collisions [20]. The suspicion that the DT should not be linearized for strong magnetic fields and small velocities is supported by a more exact numerical treatment.

4.3 PIC simulations for nonlinear dielectric response

The nonlinear Vlasov-Poisson equations (2.1–2.4) can be solved numerically. The electrons are represented by test particles in the framework of the particle-in-cell method (PIC) [22,29,30]. The applied technique is the same — except of the additional magnetic field — as described in detail in [22,30]. This PIC scheme was extensively tested for the energy loss by nonmagnetized electrons where a comparison with analytic approaches can be made in certain limiting cases. A comprehensive discussion of this comparison and evaluation is reported in [30]. In particular, the PIC results and the linearized DT well agree for weak coupling $Z\Gamma^{3/2} \ll 1$ and $\omega_c \to 0$, and both agree with the BC approach in this limit. Here the (strong) magnetic field is accounted for by employing a modified Velocity-Verlet algorithm which is based on a new resummation technique. This ensures an efficient electron/test particle propagation, where the time step is only restricted by the actual Coulomb field and not by the strength of the magnetic field, see reference [31].

As discussed above, increasing deviations between the linearized DT and the BC develop with increasing magnetic field. Already the PIC results for a moderate magnetic field with $\omega_c \approx \omega_p$, which have been presented in Figure 8 of reference [27], show that the nonlinear DT agrees rather with the second-order BC [20] than with the linearized DT. In Figure 14 we present such a comparison for a stronger magnetic field where $\omega_c \approx 100\omega_p$. The linearization of the DT yields an energy loss which is too large by more than an order of magnitude for all directions α of the ion velocity. For comoving ions, $\alpha = 0°$, the second-order BC energy loss nearly vanishes in accordance with the symmetry arguments presented above. The nonvanishing energy loss obtained from the nonlinear PIC treatment is therefore dominated by collective response.

5 Conclusions

Taking all these results together we can recommend a pragmatic approach for calculating the drag which a magnetized electron plasma exerts on an ion. Clearly the PIC solution of the nonlinear Vlasov-Poisson equation is the method of choice as it accounts for both nonlinear and dynamic collective response. For weak coupling, $Z\Gamma^{3/2} \lesssim 1$, the fluctuations inherent to the PIC simulations become large, but the second-order BC may be employed for attractive potentials or the CTMC for repulsive potentials. This neglects the collective response in a small region of

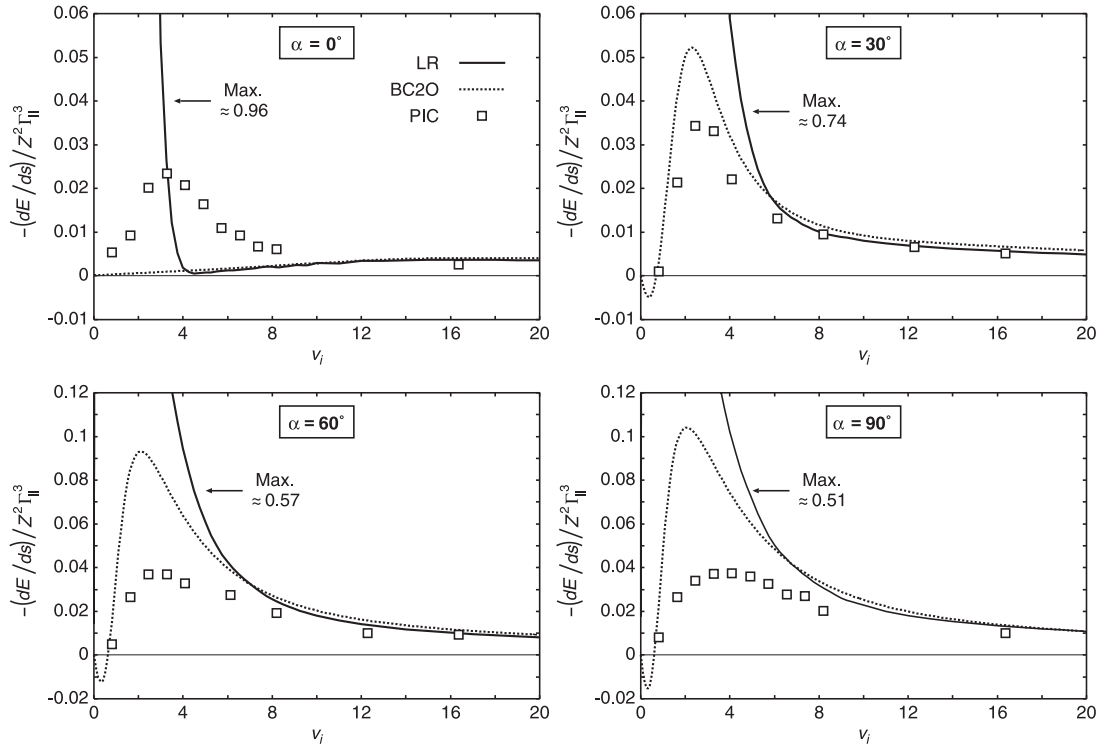

Fig. 14. Scaled energy loss as function of the scaled ion velocity. Comparison of the present linear response (LR) model (solid curves, with maximal values given), second-order binary collision (BC2O) model (dotted curves, [20]) and PIC simulations (symbols, [29]). Parameters according to set 5 of Table 3.

the ion phase space about $\alpha \approx 0°$. For large ion velocities the PIC simulations become numerically prohibitive. But there the linearized DT presented here becomes valid. Moreover, if the magnetic field is strong it can be evaluated including also the dynamic collective response.

This work has been supported by the Bundesministerium für Bildung und Forschung (BMBF 06 ER 931) and by the Gesellschaft für Schwerionenfoschung (GSI ER TO 1/2). We thank H.B. Nersisyan and P.-G. Reinhard for valuable discussions.

References

1. N. Bohr, Philos. Mag. **25**, 10 (1913); N. Bohr, Philos. Mag. **30**, 581 (1915)
2. H. Bethe, Ann. Phys. **5**, 325 (1930)
3. F. Bloch, Ann. Phys. **16**, 285 (1933)
4. E. Fermi, E. Teller, Phys. Rev. **72**, 399 (1947)
5. J. Lindhard, K. Dan. Vidensk. Selsk. Mat. Fys. Medd. **28**, 8 (1954)
6. L. de Ferraiis, A. Arista, Phys. Rev. A **29**, 2145 (1984)
7. G.I. Budker, Atomnaya Energiya **22**, 346 (1967)
8. A.H. Sørensen, E. Bonderup, Nucl. Instr. Meth. **215**, 27 (1983)
9. H. Poth, Phys. Rep. **196**, 135 (1990)
10. I.N. Meshkov, Phys. Part. Nucl. **25**, 631 (1994)
11. W. Quint, J. Dilling, S. Djekic, H. Häffner, N. Hermanspahn, H.-J. Kluge, G. Marx, R. Moore, D. Rodriguez, J. Schönfelder, G. Sikler, T. Valenzuela, J. Verdu, C. Weber, G. Werth, Hyp. Int. **132**, 457 (2001)
12. G. Gabrielse, J. Estrada, J.N. Tan, P. Yesley, N.S. Bowden, P. Oxley, T. Roach, C.H. Storry, M. Wessels, J. Tan, D. Grzonka, W. Oelert, G. Schepers, T. Sefzick, W.H. Breunlich, M. Cargnelli, H. Fuhrmann, R. King, R. Ursin, J. Zmeskal, H. Kalinowsky, C. Wesdrop, J. Walz, K.S.E. Eikema, T.W. Hänsch, Phys. Lett. B **507**, 1 (2001)
13. M. Amoretti, C. Amsler, G. Bonomi, A. Bouchta, P. Bowe, C. Carraro, C.L. Cesar, M. Charlton, M.J.T. Collier, M. Doser, V. Filippini, K.S. Fine, A. Fontana, M.C. Fujiwara, R. Funakoshi, P. Genova, J.S. Hangst, R.S. Hayano, M.H. Holzscheiter, L.V. Jørgensen, V. Lagomarsino, R. Landua, D. Lindelöf, E. Lodi Rizzini, M. Macri, N. Madsen, G. Manuzio, M. Marchesotti, P. Montagna, H. Pruys, C. Regenfus, P. Riedler, J. Rochet, A. Rotondi, G. Rouleau, G. Testera, A. Variola, T.L. Watson, D.P. van der Werf, Nature **419**, 456 (2002)
14. S. Ichimaru, *Basic Principles of Plasma Physics* (Benjamin Reading, MA, 1973), Sects. 3.4 and 7.4; S. Ichimaru, *Statistical Plasma Physics* (Addison-Wesley, Reading, MA, 1994), Vol. 1, Chap. 3 and 4
15. H.B. Nersisyan, M. Walter, G. Zwicknagel, Phys. Rev. E **61**, 7022 (2000)
16. *Handbook of Mathematical Functions*, edited by M. Abramowitz, I.A. Stegun (Dover, New York, 1972), Chap. 9

17. C. Seele, G. Zwicknagel, C. Toepffer, Phys. Rev. E **57**, 3368 (1998)
18. H.B. Nersisyan, Phys. Rev. E **58**, 3686 (1998)
19. M. Walter, Dielektrische lineare Antworttheorie magnetisierter Elektronenplasmen, thesis, Erlangen, 2003 (unpublished)
20. C. Toepffer, Phys. Rev. A **66**, 022714 (2002)
21. T. Peter, J. Meyer-ter-Vehn, Phys. Rev. A **43**, 1998 (1991)
22. G. Zwicknagel, C. Toepffer, P.-G. Reinhard, Phys. Rep. **309**, 117 (1999)
23. F.W.J. Olver, *Asymptotics and special functions* (Academic Press, New York, 1974), Chap. 2 and 3
24. M. Steinberg, J. Ortner, Phys. Rev. E **63**, 046401 (2001)
25. H.B. Nersisyan, G. Zwicknagel, C. Toepffer, Phys. Rev. E **67**, 026411 (2003)
26. B. Möllers, C. Toepffer, M. Walter, G. Zwicknagel, Nucl. Instr. Meth. B **205**, 285 (2003)
27. B. Möllers, M. Walter, G. Zwicknagel, C. Carli, C. Toepffer, Nucl. Instr. Meth. B **207**, 462 (2003)
28. G. Zwicknagel, Nucl. Instr. Meth. A **441**, 44 (2000)
29. M. Walter, C. Toepffer, G. Zwicknagel, Nucl. Instr. Meth. B **168**, 347 (2000)
30. G. Zwicknagel, Nucl. Instr. Meth. B **197**, 22 (2002)
31. Q. Spreiter, M. Walter, J. Comp. Phys. **152**, 102 (1999)